IEEE Access
Multidisciplinary | Rapid Review | Open Access Journal

Received September 24, 2021, accepted October 7, 2021, date of publication October 26, 2021, date of current version November 9, 2021.

Digital Object Identifier 10.1109/ACCESS.2021.3123180

Multi-Timescale-Based Fault Section Location in Distribution Networks

QINGLE PANG[1], LIN YE[1], HOULEI GAO[2], XINIAN LI[3], YANGJIE WANG[1], AND TONG CAO[1]

[1]School of Information and Control Engineering, Qingdao University of Technology, Qingdao 266520, China
[2]School of Electrical Engineering, Shandong University, Jinan 250061, China
[3]School of Information and Electronic Engineering, Shandong Technology and Business University, Yantai 264005, China

Corresponding author: Houlei Gao (houleig@sdu.edu.cn)

This work was supported in part by the National Natural Science Foundation of China under Grant 51877127.

ABSTRACT To meet the requirements of quickness and accuracy for fault location in smart distribution networks with high penetration of distributed generations, we propose an integrated fault section location method based on multiple timescales. On the millisecond timescale, we present a distributed fault section location method based on fault current polarity value comparison (PVC) using the first half-cycle fault current signal after the fault inception. On the cycle timescale, we implement a distributed fault section location method based on fault current waveform similarity comparison (WSC) using the first one-cycle fault current signal after the fault inception. On the second timescale, we adopt a fault section location method based on a genetic algorithm (GA) using the steady-state fault current signal. Three timescale fault section location methods thus coordinate with each other through constructed reliability functions of the fault section location methods based on PVC and WSC. The simulation results show that the multi-timescale-based fault section location method achieves a fast and accurate fault section location.

INDEX TERMS Smart distribution network, multi-timescale, integrated fault location, distributed fault section location, polarity value comparison, waveform similarity comparison, reliability function.

I. INTRODUCTION

With growing concerns about environmental issues and a looming energy crisis, the world has entered the era of sustainable energy, which is based mainly on renewable energy [1], [2]. Distributed generation (DG) is one of the main ways for renewable energy to be connected to distribution networks [3]. The modern smart distribution network, with high penetration of DG methods, is quite different from traditional distribution networks in power flow distribution, fault current amplitude, direction and distribution, which increases the complexity of fault detection and control in smart distribution networks [4]. Determining how to achieve fast fault detection, fault location, fault isolation, and fault service restoration after distribution network failure is an urgent requirement for smart distribution network self-healing [5]–[7]. Fault location is an important prerequisite and foundation of the self-healing, and determining how to achieve fault location quickly and reliably is particularly important. The fault location methods for distribution networks with DG mainly can be classified into five categories: the impedance-based method [8], [9], the traveling wave-based method [10]–[12], the signal injection-based method [13], [14], the matrix-based method [15], [16], and the artificial intelligence method [17]–[20]. The impedance-based method works based on calculating the fault loop impedance using measured currents and voltages. The method is simple and economical, but it is easily affected by an unbalanced system, nonhomogeneous conductors, and branches. The traveling-wave based method works based on the principle of transmission and reflection of the voltage (or current) traveling waves which are generated at the fault location. The main drawbacks of traveling-wave based methods are the difficulty in wave-head detection and the effect of time synchronization on the fault location accuracy. The signal injection-based method works based on the principle that the injected signal is detectable only in the section of the faulted feeder from the signal injection point to the fault point. This method requires specially designed equipment to inject a characteristic signal into the distribution systems, and the strength of the injected signal is difficult to detect. The matrix-based method works based on the current state matrix, which is constructed from

The associate editor coordinating the review of this manuscript and approving it for publication was Chenghong Gu.

the fault current state of each measuring point along the feeders. This method needs a synchronization signal to synchronize a measured current signal for distribution networks with DG. It is necessary to add a voltage transformer or global positioning system (GPS) device at each measuring point, which is cost-prohibitive. The artificial intelligence-based methods include genetic algorithms (GAs), artificial neural networks, support vector machines, fuzzy logic, and a variety of other techniques. This type of method has better fault tolerance and can be used in complex situations of multiple faults. This kind of method also has poor adaptability, however. When the power grid structure changes, it needs to update the fault location model, and the fault location time is long. The noted fault section location methods are centralized fault location methods, and their fault location strategies are formulated by the master station.

With the application of advanced technologies such as energy Internet [21] and big data in distribution networks, the master station needs to deal with a large amount of information, and the traditional centralized fault location methods are no longer suitable for smart distribution networks. At the same time, these advanced technologies make it possible to realize distributed control by the smart distribution unit (SDU), such as feeder terminal unit (FTU) and distribution terminal unit. The smart distribution network requires the SDU not only to have the function of data acquisition, but also to have the functions of fault detection, fault location, fault isolation, and fault service restoration. It is urgent to study the distributed fault location method based on the smart distribution terminal. Sun *et al.* [22] proposed the fault section location based on FTU in the distribution network with DGs by means of time coordination between the current quick-break protection and the time-limited overcurrent protection set at the upstream and downstream measuring points of the DG. This method needed to calculate only the amplitude of the fault currents, without distinguishing their directions, but the relay protection configuration was complex, the fault section location time was long, and the adaptability to various grid structures was poor, which could not meet the requirements of smart distribution networks. To meet the requirements of smart distribution networks for the rapidity of fault location, we proposed two fast distributed fault section location methods: the fault section location method based on fault current polarity value comparison (PVC) using the first half-cycle fault current signal and the fault section location method based on fault current waveform similarity comparison (WSC) using the first one-cycle fault current signal. Although these two distributed fault section location methods could achieve fast fault location, fault location errors would occur when fault characteristics were not significant, and their fault tolerance was weak. To meet the requirements of smart distribution networks for the accuracy of fault location, we fused a fault section location method based on GAs with the two distributed fault location methods and proposed an integrated fault section location method for smart distribution networks based on millisecond timescale, cycle timescale, and second timescale.

The contribution of this work is summarized as follows:

- We proposed the distributed fault section location method based on fault current PVC. The method is implemented by SDUs through information interaction with their adjacent smart distribution terminals and only uses the first half-cycle fault current signal after the fault inception. This fault section location method can provide ultrafast fault location.
- We proposed the distributed fault section location method based on fault current WSC. This method is also implemented by SDUs and uses the first one-cycle fault current signal after the fault inception. This fault section location method can realize fast fault location.
- To complement the PVC-based method, the WSC-based method, and the GA based method, we established the reliability functions of the PVC- and WSC-based fault section location methods. These fault section location methods can coordinate with each other by means of these reliability functions to realize fast and accuracy fault section location.
- We verified the proposed integrated fault section location using simulation and field fault current data. The results verified the proposed integrated fault section location method can provide fast and accurate fault section location for short-circuit faults.

The remainder of this paper is organized as follows. Section II proposes the millisecond timescale fault section location method based on PVC. Section III introduces the cycle timescale fault section location based on WSC. Section IV analyzes the problems of the distributed fault locations based on PVC and WSC. Section V reports the integrated fault section location method based on multiple timescales. Section VI and section VII discusses the simulation and field results, respectively. Section VIII presents the conclusion and future work.

II. PVC-BASED MILLISECOND TIMESCALE FAULT SECTION LOCATION METHOD

A. DISTRIBUTED FEEDER AUTOMATION SYSTEM

The simple structure of distributed feeder automation (FA) suitable for smart distribution networks is shown in Fig. 1. Under normal operation, the section switch is closed and the tie switch is open. The master station and SDU interact with each other through the communication network. Each SDU carries out distributed control according to the collected local information and the interaction information with other devices, so as to achieve fault location, fault isolation, and fault service restoration.

B. PRINCIPLE OF FAULT SECTION LOCATION

The principle of fault section location based on PVC is that the polarities of the measured fault currents on both sides of fault section are opposite, whereas those on each side

of the sound section are the same. The traditional current polarity comparison methods need to collect a cycle of the fault current signal, then use fast Fourier transformation to calculate the phase of the fault current signal, and then compare with the fault current phase of other nodes to achieve the fault section location. These methods are complex in calculation, time-consuming, and require accurate synchronization of data, so they are not applicable to fault section location in distributed FA with SDU.

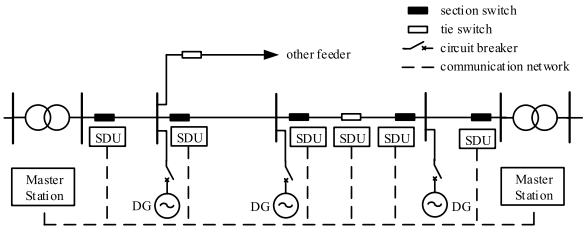

FIGURE 1. Simple diagram of distributed feeder automation.

Because the inception information of the fault current signal can accurately reflect the fault characteristics, to simplify the fault location algorithm and achieve fast fault location, the polarity of the fault current is judged by calculating the polarity value of the half-cycle fault current signal after the fault inception time. If there is a zero-crossing point in the half-cycle fault current, the data between the fault inception time and the zero-crossing point are taken as the half-cycle fault current signal. The polarity value is defined as the number of samples with positive or negative values in the specified data window. The polarity value of fault current at a detection point is defined as follows:

$$PN = \begin{cases} M\,\mathrm{sign}(i(1)), & \mathrm{sign}(i(M)\cdot i(M+1)) \le 0, \\ & M \in [1,\ N) \\ 0, & \mathrm{non-fault} \\ N\,\mathrm{sign}(i(1)), & \mathrm{sign}(i(m)\cdot i(m+1)) = 1, \\ & \forall m \in [1,\ N), \end{cases} \tag{1}$$

$$\mathrm{sign}(x) = \begin{cases} 1, & x > 0 \\ 0, & x = 0 \\ -1, & x < 0, \end{cases} \tag{2}$$

where PN is the polarity value of fault current at the detection point; $PN \ge 0$ indicates that the polarity of fault current is positive, otherwise it is negative; $\mathrm{sign}(x)$ is a symbolic function; $i(m)$ is the m^{th} sampling value of the fault current at the detection point; M is the sequence number at which the fault current sampling data first crosses the zero point in the half-cycle; and N is the number of sampling points in half-cycle.

The SDU judges whether the section is a fault section according to the polarity value difference and the polarity value sum of fault currents between the upstream and downstream detection points. The fault section location criterion is that the polarity value of fault current between two adjacent detection points meets the following formula; if so, then the section between two detection points is a fault section:

$$\begin{cases} |PND| - k_{\mathrm{res}}\,|PNS| \ge k_{\mathrm{re}} D_{\mathrm{th}} \\ PND = PN_{\mathrm{u}} - PN_{\mathrm{d}} \\ PNS = PN_{\mathrm{u}} + PN_{\mathrm{d}}, \end{cases} \tag{3}$$

where PND is the difference of fault current polarity values between upstream and downstream detection points; PNS is the sum of fault current polarity values between upstream and downstream detection points; D_{th} is the threshold, $D_{\mathrm{th}} = \min(|PN_u|, |PN_d|)$; k_{re} is the reliability coefficient, which is generally taken as $0.1 < k_{\mathrm{re}} < 0.3$; k_{res} is the restraint coefficient, which is generally taken as $0.8 < k_{\mathrm{res}} < 1.2$; and PN_u and PN_{d} are the polarity values at upstream detection point u and downstream detection point d respectively. When there is no downstream detection point or the polarity value at the downstream detection point is 0, if the following formula is satisfied, the section after the detection point is a fault section:

$$|PND| \ge k_{\mathrm{re}} D_{\mathrm{th}}. \tag{4}$$

C. STARTING CRITERION OF FAULT SECTION LOCATION

The traditional starting criterion of the fault section location is that the effective value of the fault current exceeds a threshold. However, it takes tens of milliseconds to calculate the effective value of the fault current, which leads to the slow speed of fault section location. To increase the speed of fault location, we took the current sudden changes as the starting criterion.

The SDU detects the phase current at each detection point in real time. To avoid a false start caused by interference, the variations of three consecutive current sampling values are calculated to judge whether the distribution network has failed. When the changes of three consecutive sampling values of a line current meet the following formula, the short-circuit fault location is started:

$$\begin{cases} \left|i_{\mathrm{p}}(k) - i_{\mathrm{p}}(k-2N)\right| \ge k_{\mathrm{sp}} I_{\mathrm{p}} \\ \left|i_{\mathrm{p}}(k) - i_{\mathrm{p}}(k-2N)\right| \ge k_{\mathrm{ip}} \left|i_{\mathrm{p}}(k-2N)\right|, \end{cases} \tag{5}$$

where $i_{\mathrm{p}}(k)$ is the k^{th} sampling value of phase current; $i_{\mathrm{p}}(k-2N)$ is the sampling value of phase current of the previous cycle at the k^{th} sampling point, and the number of one-cycle sampling points is $2N$; k_{sp} is the constraint factor of phase current, which is generally taken as $0.2 < k_{\mathrm{sp}} < 0.4$; k_{ip} is the scale factor of phase current, which is generally taken as $2 < k_{\mathrm{ip}} < 4$; and I_{p} is the effective value of the normal load current at the detection point.

When the starting criterion of formula (5) is met, each SDU takes the k^{th} sampling point as the fault inception point, and records the first half-cycle fault current signal after the fault. Then, each SDU calculates the fault current polarity value of the local detection point using formulas (1) and (2), and receives the fault current polarity value of its downstream detection point through the downstream SDU. Thus, each SDU can judge whether the section between the local detection point and the downstream detection point is a fault

section based on formula (3) or (4). When a section fails, the fault current polarity values at the two ends of the downstream section with a DG will meet the criteria put forward in formula (4), and the downstream section will be misjudged as a failed section. Therefore, when the upstream section has been confirmed as the fault section, all the downstream fault section location results are canceled.

III. WSC-BASED CYCLE TIMESCALE FAULT SECTION LOCATION

A. PRINCIPLE OF FAULT SECTION LOCATION

The principle of fault section location based on WSC is that the fault current waveforms on both sides of the fault section are quite different, whereas those on each side of the sound section are quite similar. The correlation coefficient method is the simplest and most effective method to compare the similarity between the two waveforms. The similarity is judged by calculating the correlation coefficient between the fault currents of two adjacent detection points. The formula for calculating the fault current correlation coefficient ρ_{ud} between upstream and downstream detection points u and d is as follows:

$$\rho_{ud} = \frac{\sum_{k=1}^{2N} i_u(k) i_d(k)}{\sqrt{\sum_{k=1}^{2N} i_u^2(k) \sum_{k=1}^{2N} i_d^2(k)}}, \tag{6}$$

where $i_u(k)$ and $i_d(k)$ are the k^{th} sampling values of the fault currents of upstream and downstream detection points u and d, respectively, and $2N$ is the number of sampling points during one power cycle.

The fault section location criterion is that the section between two adjacent detection points is the fault section if the similarity of their fault currents meets the following formula.

$$\rho_{ud} < \rho_{set}, \tag{7}$$

where ρ_{set} is the correlation coefficient threshold, which generally is taken as 0.6–0.8.

Formula (5) is still used as the starting criterion for fault section location. When the starting criterion is met, each SDU stores the first cycle fault current signal, and informs the downstream SDU to upload its first cycle fault current signal. Each SDU calculates the correlation coefficient of fault currents between the local detection point and its downstream detection point according to formula (6), and judges whether the section between the adjacent detection points is a fault section according to formula (7). When a section fails, the current waveforms at the two ends of the downstream section with a DG will meet the formula (7), and the downstream section will be misjudged as a failed section. Therefore, when the upstream section has been confirmed as the fault section, all the downstream fault section location results are canceled.

B. FAULT STARTING TIME CORRECTION

When using formula (6) to calculate the correlation coefficient, if the two fault inception times judged by the upstream and downstream SDU are the same, the fault currents detected at the adjacent detection points are completely synchronized, and the calculated correlation coefficient can accurately express the similarity of the two fault current waveforms. Because of limited sampling accuracy, the difference of current amplitude, and the influence of interference factors, the judged fault inception times at adjacent detection points are not consistent, resulting in two asynchronous fault currents detected at adjacent detection points. As a result, the calculated correlation coefficient will be inaccurate and the result of fault section location will be wrong. Therefore, it is necessary to correct the fault inception sampling data of adjacent detection points. If the SDU is equipped with a GPS synchronous clock, the fault current signal at the detection point can be added with a time stamp, and the fault inception point can be corrected according to the time stamp. If the SDU is not equipped with a GPS synchronous clock, the correlation coefficient is calculated as follows. The fault current data window of the local detection point is taken as a benchmark, the fault current data window of the downstream detection point is shifted to the left and right of each sampling point, and the maximum shifting data length is 1/16 power cycle (i.e., 1.25 ms). The correlation coefficient between two adjacent detection points after each shift is calculated, and the maximum and minimum values of all correlation coefficients are recorded. If the correlation coefficient is relatively large (i.e., greater than 0.5), the maximum correlation coefficient is taken as the final correlation coefficient of the two adjacent detection points, namely:

$$\rho_{udmax} = \max_{j=-N/8}^{N/8} \rho_{ud}(j) = \max_{j=-N/8}^{N/8} \frac{\sum_{k=1}^{2N} i_u(k) i_d(k+j)}{\sqrt{\sum_{k=1}^{2N} i_u^2(k) \sum_{k=1}^{2N} i_d^2(k+j)}}, \tag{8}$$

where $i_u(k)$ is the k^{th} fault current sampling value of the local detection point u; $i_d(k+j)$ is the $(k+j)^{th}$ fault current sampling value of the downstream detection point d; $2N$ is the number of sampling points of one power cycle; and j is the data shifting length.

If the correlation coefficient is relatively small (i.e., less than 0.5), the minimum correlation coefficient is taken as the final correlation coefficient of the two adjacent detection points, namely:

$$\rho_{udmin} = \min_{j=-N/8}^{N/8} \rho_{ud}(j) = \min_{j=-N/8}^{N/8} \frac{\sum_{k=1}^{2N} i_u(k) i_d(k+j)}{\sqrt{\sum_{k=1}^{2N} i_u^2(k) \sum_{k=1}^{2N} i_d^2(k+j)}}. \tag{9}$$

IV. PROBLEM OF DISTRIBUTED FAULT SECTION LOCATION

These fault section location methods based on PVC and WSC are implemented by the distributed SDU, which belong to the distributed fault location method and has fast fault location speed. The PVC-based fault section location method uses only half-cycle transient fault current data, and the fault section location time is less than 20 ms. The WSC-based fault section location method uses only the one-cycle transient fault current data, and the fault section location time is less than two cycles (i.e., 40 ms). If, however, the fault current signals are disturbed or out of synchronization, the fault section location results may be wrong.

A feeder with four detection points is shown in Fig. 2, and the short-circuit currents at these detection points are i_1, i_2, i_3, and i_4. We assumed a phase-phase short-circuit fault occurred at k in section II. The short-circuit current waveforms of A-phase at the detection points 1, 2, and 3 are shown in Fig. 3. Using formulas (3) and (6), *PND*, *PNS,* and ρ could be calculated. The coefficients were set as following: $k_{\text{res}} = 1$, $k_{\text{re}} = 0.2$, $\rho_{\text{set}} = 0.7$. Using the formula (3) and (7), the fault section location results based on PVC and WSC could be achieved, as shown in Table 1. Table 1 shows that the fault section was in section II and the fault section location results based on PVC and WSC were correct.

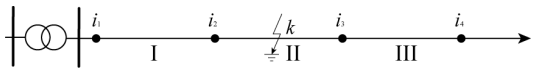

FIGURE 2. Simple diagram of distributed feeder automation.

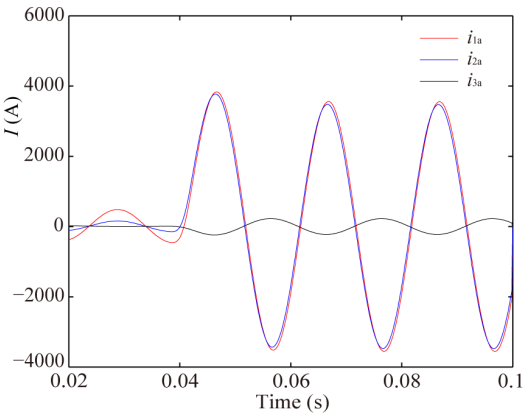

FIGURE 3. Waveform of A-phase fault currents.

TABLE 1. Fault section location results.

Section	Current	PVC				WSC	
		PND	*PNS*	D_{th}	Fault location	ρ	Fault location
I	i_{1a}, i_{2a}	0	128	64	Sound	0.9932	Sound
II	i_{2a}, i_{3a}	128	0	64	Fault	-0.9693	Fault

Figure 4 shows the system assuming that the short-circuit current i_{3a} had an interference signal. The fault section location results based on PVC and WSC are given in Table 2. Table 2 shows that the fault section location result based on PVC was incorrect. Thus, when the fault current signals are disturbed, the fault section location results based on PVC may be invalid.

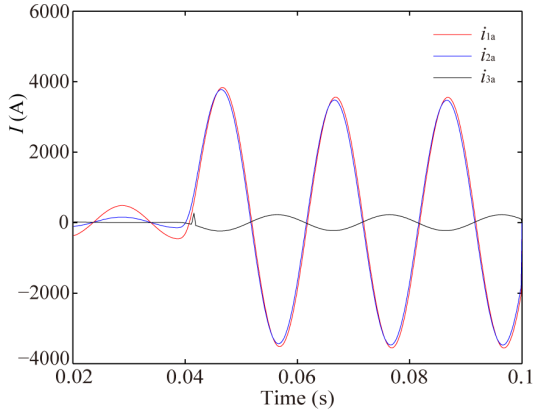

FIGURE 4. Waveform of A-phase fault currents with interference.

TABLE 2. Fault section location results with interference.

Section	Current	PVC				WSC	
		PND	*PNS*	D_{th}	Fault location	ρ	Fault location
I	i_{1a}, i_{2a}	0	128	64	Sound	0.9932	Sound
II	i_{2a}, i_{3a}	61	-67	3	Sound	-0.9136	Fault
III	i_{3a}, i_{4a}	3	3	0	Fault	0	Sound

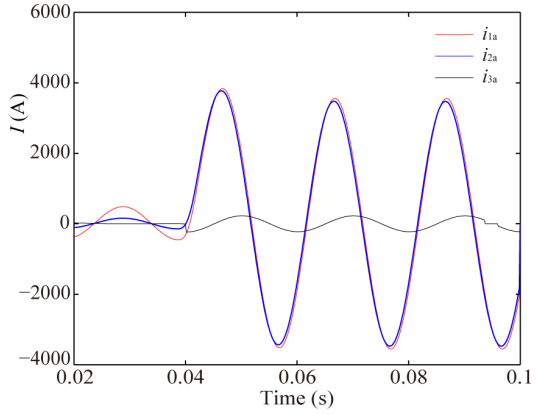

FIGURE 5. Waveform of A-phase fault currents with time lag.

Figure 5 shows the system assuming that the short-circuit current i_{3a} was lagged for some time. We used the fault section location methods based on PVC and WSC, and the fault section location results are given in Table 3. Table 3 shows that the fault section location result based on WSC was incorrect. Thus, when the fault current signals between adjacent detection points are not synchronized, the fault section location results based on WSC may be invalid.

V. MULTI-TIMESCALE-BASED FAULT SECTION LOCATION METHOD

The timescales of these three fault section location methods are different: the fault section location speed of the

TABLE 3. Fault section location results with time lag.

Section	Current	PVC				WSC	
		PND	*PNS*	D_{th}	Fault location	ρ	Fault location
I	i_{1a}, i_{2a}	0	128	64	Sound	0.9932	Sound
II	i_{2a}, i_{3a}	97	31	33	Fault	0.3222	Sound
III	i_{3a}, i_{4a}	-33	-33	0	Sound	0	Fault

PVC-based method is the fastest and that of the GA-based method is the slowest. To achieve fast fault location, the PVC-based fault location method is preferred. Because of the difference of the fault location, fault impedance, fault time, and fault duration, the collected fault currents are different, the fault features collected by different fault location methods are different, and the reliabilities of fault location results based on different fault location methods are also different. To achieve an accurate and fast fault location result, we analyzed the reliability of each fault location method and defined the reliability functions for distributed fault location methods to make them cooperate closely.

A. RELIABILITY ANALYSIS OF PVC-BASED METHOD

When calculating the polarity value of fault current using formula (1), the larger the amplitude of the detected fault current is, the higher the reliability of the fault current polarity value is. Therefore, the reliability function T_{PNp} of fault phase current polarity value is defined as follows:

$$T_{\mathrm{PNp}} = \begin{cases} 0, & I_{\mathrm{kp}} < k_{\mathrm{skp}} I_{\mathrm{p}} \\ \dfrac{I_{\mathrm{kp}} - k_{\mathrm{skp}} I_{\mathrm{p}}}{(k_{\mathrm{stkp}} - k_{\mathrm{skp}}) I_{\mathrm{p}}}, & k_{\mathrm{skp}} I_{\mathrm{p}} \le I_{\mathrm{kp}} < k_{\mathrm{stkp}} I_{\mathrm{p}} \\ 1, & I_{\mathrm{kp}} \ge k_{\mathrm{stkp}} I_{\mathrm{p}}, \end{cases} \tag{10}$$

where I_{kp} is the effective value of fault phase current; I_{p} is the effective value of sound phase current; k_{skp} is the constraint coefficient of fault phase current, which is generally taken as 1.5–2; and k_{stkp} is the reliability coefficient of fault phase current polarity value, which is generally taken as 5–7.

The larger the polarity value difference between adjacent detection points is, the higher the reliability of the fault section location result is. Thus, the reliability function T_{PR} of the current PVC is defined as follows:

$$T_{\mathrm{PR}} = \begin{cases} 0, & |PND| - k_{\mathrm{res}} |PNS| < k_{\mathrm{re}} D_{\mathrm{th}} \\ \dfrac{|PND| - k_{\mathrm{res}} |PNS|}{B}, & k_{\mathrm{re}} D_{\mathrm{th}} \le |PND| - k_{\mathrm{res}} |PNS| < B \\ 1, & |PND| - k_{\mathrm{res}} |PNS| \ge B, \end{cases} \tag{11}$$

where $B = \max(|PN_u|, |PN_d|)$.

When the fault current duration is less than a half-cycle, the reliability of fault location result will be reduced. Therefore, the fault current reliability function T_{PI} is defined as follows:

$$T_{\mathrm{PI}} = \begin{cases} \dfrac{t_{\mathrm{kend}} - t_{\mathrm{kstart}}}{0.01}, & 0 \le t_{\mathrm{kend}} - t_{\mathrm{kstart}} < 0.01 \\ 1, & t_{\mathrm{kend}} - t_{\mathrm{kstart}} \ge 0.01 \end{cases} \tag{12}$$

where t_{kstart} is the fault inception time; and t_{kend} is the fault end time.

According to the reliability function of the current polarity value, the reliability function of the PVC, and the reliability function of fault current, the PVC-based fault section location reliability function T_{P} is defined as follows:

$$T_{\mathrm{P}} = T_{\mathrm{PI}}(T_{\mathrm{PN}} + T_{\mathrm{PR}})/2, \tag{13}$$

where T_{PN} is the reliability function of the current polarity values of detection points; T_{PR} is the reliability function of the PVC of detection points; and T_{PI} is the reliability function of fault current of detection points.

If there is no downstream detection point or the polarity value at the downstream detection point is 0, the PVC-based fault section location reliability function T_{P} is defined as follows:

$$T_{\mathrm{P}} = T_{\mathrm{PI}} T_{\mathrm{PN}}. \tag{14}$$

B. RELIABILITY ANALYSIS OF PVC-BASED METHOD

When calculating the fault current similarity between two adjacent detection points using formula (6), the larger the fault current amplitude is, the higher the reliability of the calculated similarity is. The defined similarity reliability function T_{WSp} is the same as the fault current polarity reliability function T_{PNp} (i.e., $T_{\mathrm{WSp}} = T_{\mathrm{PNp}}$). At the same time, when judging the fault location using formula (7), the smaller ρ_{ud} is, the higher the reliability of the fault location result is. Thus, the reliability function T_{WR} of the WSC is defined as follows:

$$T_{\mathrm{WR}} = \begin{cases} 0, & \rho_{\mathrm{ud}} > \rho_{\mathrm{set}} \\ \dfrac{\rho_{\mathrm{set}} - \rho_{\mathrm{ud}}}{\rho_{\mathrm{set}}}, & 0 < \rho_{\mathrm{ud}} \le \rho_{\mathrm{set}} \\ 1, & \rho_{\mathrm{ud}} \le 0. \end{cases} \tag{15}$$

When the fault current duration is less than one cycle, the reliability of fault location result will be reduced. Therefore, the fault current reliability function T_{WI} is defined as follows:

$$T_{\mathrm{WI}} = \begin{cases} \dfrac{t_{\mathrm{kend}} - t_{\mathrm{kstart}}}{0.02}, & 0 \le t_{\mathrm{kend}} - t_{\mathrm{kstart}} < 0.02 \\ 1, & t_{\mathrm{kend}} - t_{\mathrm{kstart}} > 0.02, \end{cases} \tag{16}$$

where t_{kstart} is the fault inception time; and t_{kend} is the fault end time.

According to the reliability function of fault phase current similarity, the reliability function of the WSC, and the reliability function of fault current, the WSC-based fault section location reliability function T_{W} is defined as follows:

$$T_{\mathrm{W}} = T_{\mathrm{WI}}(T_{\mathrm{WS}} + T_{\mathrm{WR}})/2, \tag{17}$$

where T_{WS} is the similarity reliability function of detection points; T_{WR} is the reliability function of WSC of detection points; and T_{WI} is the reliability function of fault current.

If there is no downstream detection point or fault currents are not detected at the downstream detection point, the WSC-based fault section location reliability function T_{W} is defined as follows:

$$T_{\mathrm{W}} = T_{\mathrm{WI}} T_{\mathrm{WS}}. \tag{18}$$

C. MULTI-TIMESCALE-BASED FAULT SECTION LOCATION

To meet the requirements of quickness and accuracy for fault location in smart distribution networks, it is necessary to effectively coordinate the three fault location methods. Following the principle of three-stage current protection, we defined the multi-timescale-based fault section location method as follows: the millisecond timescale PVC-based fault section location method is regarded as the first-stage fault section location method, the cycle timescale WSC-based fault section location method is taken as the second-stage fault section location method, and the second timescale GA-based fault section location is seen as the third-stage fault section location method.

The reliability of the fault section location result is related to the richness of fault information obtained by fault location methods. In general, the third-stage fault section location results had the highest results, followed by the second-stage fault section location. The first-stage fault section location had the lowest results. The first-stage fault section location was the fastest, followed by the second-stage fault section location, and the third-stage fault section location was the slowest. Thus, the three fault section location methods were coordinated in the following ways: first, start the first-stage fault location. If the T_{P} calculated by formula (13) or (14) satisfies $T_{\mathrm{P}} > T_{\mathrm{Pth}}$, where T_{Pth} is the fault reliability threshold for the PVC-based method, the reliability of the first-stage fault location result is higher, and the first-stage location outputs the fault location result. In this case, other fault section locations will not be started. If $T_{\mathrm{P}} > T_{\mathrm{Pth}}$ is not satisfied, the second-stage location is started, and if the T_{W} calculated by formula (17) or (18) satisfies $T_{\mathrm{W}} > T_{\mathrm{Wth}}$, where T_{Wth} is the fault reliability threshold for WSC-based method, the reliability of the second-stage location result is higher. In this case, the second stage location outputs the fault location result, and the third-stage location will not be started. Finally, when the reliability of the first-stage and second-stage location results are both low, the third-stage location is started.

The flowchart of the multi-timescale-based fault location is shown in Fig. 6. Following are the steps of the new fault section location method:

1. The distributed SDUs in distribution networks acquire the three phase currents in real time. When the starting criterion is met by formula (5), start the PVC-based fault section location process.
2. The SDU collects the half-cycle fault phase current and calculates *PN* by formula (1). Obtain *PN* of the downstream detection point and calculate *PND* and *PNS* by formula (3). If the PVC-based fault section location criterion is met by formula (3) or formula (4) and the fault section location reliability function T_{P} is greater than its threshold, output the fault section location results. Otherwise, perform the SWC-based fault section location process.
3. The SDU collects the one-cycle fault phase current and obtains the one-cycle fault phase current of the downstream detection point. Calculate ρ_{ud} by formula (6) and update ρ_{ud} by formula (8) or formula (9). If the SWC-based fault section location criterion is met by formula (7) and the fault section location reliability function T_{W} is greater than its threshold, output the fault section location results. Otherwise, perform the GA-based fault section location process.
4. The master station performs the GA-based fault section location process.

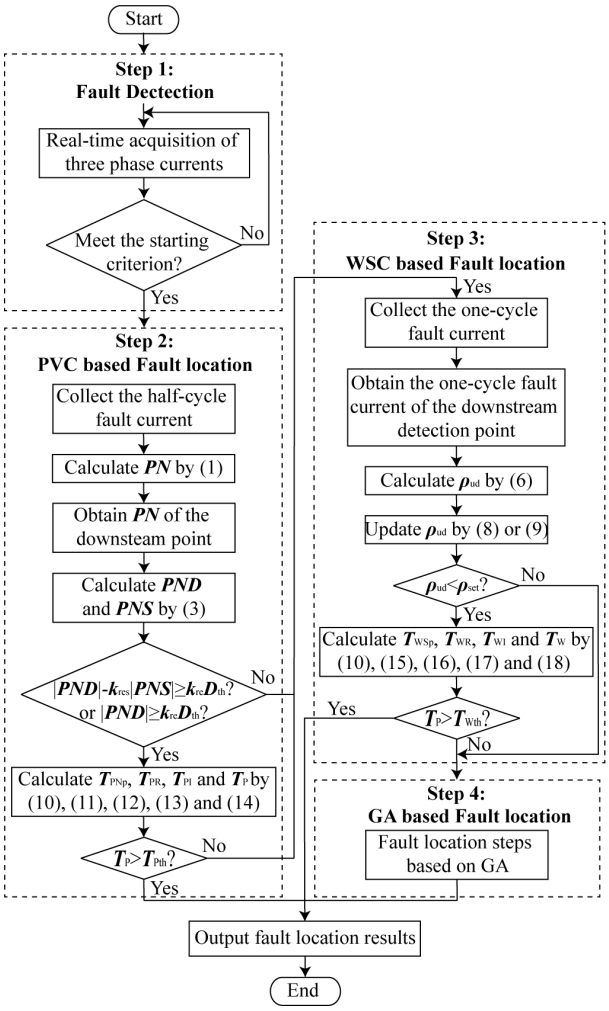

FIGURE 6. Flowchart of the multi-timescale-based fault location.

VI. SIMULATION ANALYSIS

A. SIMULATION MODEL

The simulation model for a typical 10 kV distribution system based on EMTP/ATP is shown in Fig. 7. The system has six feeders, and the feeders are hybrid lines containing overhead lines and cable lines. D_1, D_2, D_3, and D_4 are the four detection points of feeder L_4. I, II, III, and IV are the sections between D_1 and D_2, D_2 and D_3, D_3 and D_4, and D_4 and the end, respectively; i_{ja}, i_{jb}, and i_{jc} ($j = 1, 2, 3, 4$) are the three phase currents in the detection point D_j. The parameters of overhead lines and cable lines are shown in Table 4. The loads are all connected in a triangle, and the

impedance $Z_L = (67 + j50)\ \Omega$. The DG can be regarded as a constant current source with the rated current of 300 A during the normal operation of distribution networks. When a fault occurs, it is a controlled current source whose current changes with the positive sequence voltage of the access point, and its constraint current multiple is set to 2.

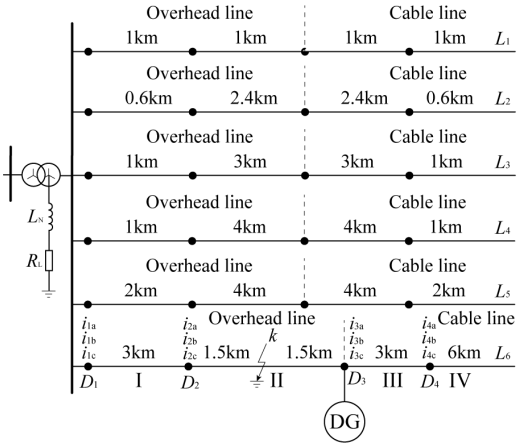

FIGURE 7. Simulation model of distribution network.

TABLE 4. Feeder parameters.

Line type	Phase-sequence	R (Ω/km)	L (Ω/km)	C (μS/km)
Overhead line	Positive-sequence	0.17	0.38	3.099
	Zero-sequence	0.23	1.72	2.477
Cable line	Positive-sequence	0.28	0.083	106.76
	Zero-sequence	2.8	0.32	91.06

B. SIMULATION VERIFICATION FOR THE PVC- AND WSC-BASED FAULT SECTION LOCATION METHOD

We verified this fault location method by a three-phase short-circuit fault and a phase-phase short-circuit fault (A-B phase) at k point in section II of the L_6. The sampling frequency was set to 6.4 kHz in the system (i.e., 128 sampling points were collected per power cycle). In the PVC-based fault location method, 64 sampling points from the fault inception time were collected; 128 sampling points from the fault inception time were collected in the WSC-based fault location method; and 128 sampling points during 641–768 after the fault were collected in the GA-based fault location method. In the process of fault section location, $k_{res} = 1$, $k_{re} = 0.2$, $\rho_{set} = 0.7$, $k_{skp} = 1.8$, $k_{stkp} = 6$, and $T_{Pth} = T_{Wth} = 0.6$. The simulations were carried out on the following cases:

- Fault type: three-phase short-circuit fault and phase-phase short-circuit fault
- Fault position: 1.5 km, 4.5 km, 7.5 km, 10.5 km from fault point to bus in the feeder L_6
- Fault resistance: 0, 0.1, 0.2, 1, 5, 10
- Fault inception angle: 0°, 10°, 30°, 45°, 90°

Thus, we obtained 240 sets of fault data.

1) THREE-PHASE SHORT-CIRCUIT FAULT

The fault currents and voltage of the A-phase for the three-phase short-circuit fault with fault inception angle (φ_f) of 10°, fault resistance (R_f) of 0.1 Ω and fault position of 4.5 km are shown in Fig. 8. Using formula (5), we judged that three-phase short-circuit faults occurred and the fault section location process was started. Using formulas (3) and (6), the fault location parameters *PND*, *PNS*, and ρ for the PVC-based and WSC-based fault section location could be calculated, and their fault section location results were achieved using formulas (3) and (7). Some calculation results of A-phase for fault position of 4.5 km are shown in Table 5, where i_{1a}, i_{2a}, i_{3a}, and i_{4a} were the A-phase fault currents of the detection points D_1, D_2, D_3, and D_4, respectively. All fault section location results were correct, and the fault location results based on PVC and WSC were not affected by DG.

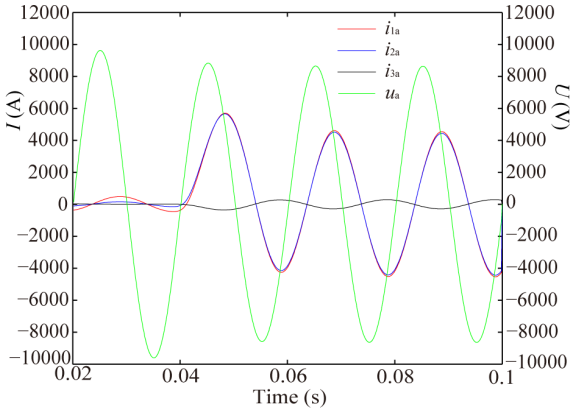

FIGURE 8. Fault currents and voltage of A-phase for three-phase short circuit.

Using formulas (13) and (17), the PVC-based and WSC-based fault section location reliability could be calculated, as shown in Table 5, where "—" indicates that the section was not the fault section and, correspondingly, its fault section location reliability need not be calculated. Table 5 shows that the PVC-based and WSC-based fault section location reliabilities of all fault types were greater than 0.6: the fault section location reliability for all kinds of faults was high.

2) PHASE-PHASE SHORT-CIRCUIT FAULT

After a phase-phase short-circuit fault occurred, the fault section location process was started using formula (5). Using formulas (3) and (6), the fault location parameters *PND*, *PNS,* and ρ for the PVC-based and WSC-based fault section location were calculated, and their fault section location results were achieved using formulas (3) and (7). Some calculation results of A-phase with fault position of 4.5 km are shown in Table 6. In Table 6, all fault section location results were correct except for the fault with fault resistance of 10 Ω and fault inception angle of 90°. The accuracy of fault section location was 96.67% for the PVC-based and WSC-based fault section location methods in the 120 fault cases corresponding to a phase-phase short-circuit fault. The fault section location results could be achieved using GA for the short-circuit faults, whereas the fault location results are incorrect using the PVC and WSC methods.

TABLE 5. PVC-based and WSC-based fault section location results for three-phase short-circuit fault.

Fault type		Section	Current	PVC					WSC		
Fault inception angle φ_f (°)	Fault resistance R_f (Ω)			*PND*	*PNS*	D_{th}	Fault location result	T_P	ρ	Fault location result	T_W
10	0.1	I	i_{1a}, i_{2a}	0	128	64	Sound	—	0.9823	Sound	—
		II	i_{2a}, i_{3a}	128	0	64	Fault	1	-0.9544	Fault	1
		III	i_{3a}, i_{4a}	-64	-64	0	Sound	—	0	Sound	—
	10	I	i_{1a}, i_{2a}	0	128	64	Sound	—	0.9955	Sound	—
		II	i_{2a}, i_{3a}	118	10	54	Fault	0.7149	-0.8133	Fault	0.7125
		III	i_{3a}, i_{4a}	-54	-54	0	Sound	—	0	Sound	—
45	0.1	I	i_{1a}, i_{2a}	0	128	64	Sound	—	0.9927	Sound	—
		II	i_{2a}, i_{3a}	128	0	64	Fault	1	-0.9487	Fault	1
		III	i_{3a}, i_{4a}	-64	-64	0	Sound	—	0	Sound	—
	10	I	i_{1a}, i_{2a}	0	120	60	Sound	—	0.9996	Sound	—
		II	i_{2a}, i_{3a}	108	12	48	Fault	0.6889	-0.8152	Fault	0.6997
		III	i_{3a}, i_{4a}	-47	-48	0	Sound	—	0	Sound	—
90	0.1	I	i_{1a}, i_{2a}	-2	116	57	Sound	—	0.9950	Sound	—
		II	i_{2a}, i_{3a}	110	8	51	Fault	1	-0.9087	Fault	1
		III	i_{3a}, i_{4a}	-51	-51	0	Sound	—	0	Sound	—
	10	I	i_{1a}, i_{2a}	-1	89	44	Sound	—	0.9926	Sound	—
		II	i_{2a}, i_{3a}	77	13	32	Fault	0.6151	-0.7724	Fault	0.6660
		III	i_{3a}, i_{4a}	-32	-32	0	Sound	—	0	Sound	—
45 (with interference)	0.1	I	i_{1a}, i_{2a}	67	61	3	Fault	0.5469	0.9925	Sound	—
		II	i_{2a}, i_{3a}	61	-67	3	Sound	—	-0.9479	Fault	1
		III	i_{3a}, i_{4a}	-64	-64	0	Sound	—	1	Sound	—

TABLE 6. PVC-based and WSC-based fault section location results for phase-phase short-circuit fault.

Fault type		Section	Current	PVC					WSC		
Fault inception angle φ_f (°)	Fault resistance R_f (Ω)			*PND*	*PNS*	D_{th}	Fault location result	T_P	ρ	Fault location result	T_W
45	0.1	I	i_{1a}, i_{2a}	0	128	64	Sound	—	0.9949	Sound	—
		II	i_{2a}, i_{3a}	122	6	58	Fault	1	-0.9332	Fault	1
		III	i_{3a}, i_{4a}	-58	-58	0	Sound	—	0	Sound	—
	10	I	i_{1a}, i_{2a}	1	103	51	Sound	—	0.9967	Sound	—
		II	i_{2a}, i_{3a}	89	13	38	Fault	0.5775	-0.7523	Fault	0.6059
		III	i_{3a}, i_{4a}	-38	-38	0	Sound	—	0	Sound	—
90	0.1	I	i_{1a}, i_{2a}	-1	85	42	Sound	—	0.9935	Sound	—
		II	i_{2a}, i_{3a}	76	10	33	Fault	0.8749	-0.8597	Fault	1
		III	i_{3a}, i_{4a}	-33	-33	0	Sound	—	0	Sound	—
	10	I	i_{1a}, i_{2a}	-3	65	31	Sound	—	0.9770	Sound	—
		II	i_{2a}, i_{3a}	-13	81	34	Sound	—	0.7472	Sound	—
		III	i_{3a}, i_{4a}	47	47	0	Fault	0	0	Fault	0

Using formulas (13) and (17), the PVC-based and WSC-based fault section location reliability was calculated, as shown in Table 6. Table 6 shows that the PVC-based and WSC-based fault section location reliabilities were greater than 0.6, except for the following two cases: when the fault resistance was 10 Ω and the fault inception angle was 45°, and when the fault resistance was 10 Ω and the fault inception angle was 90°.

C. SIMULATION VERIFICATION FOR MULTI-TIMESCALE-BASED FAULT SECTION LOCATION METHOD

After a short-circuit fault occurred, the PVC-based first-stage fault section location was started. Using formula (3), the fault section location result was achieved. Then the fault section location reliability of the PVC-based fault location was calculated using formula (13). If $T_P > T_{Pth}$, such as in the case of the three-phase short-circuit fault with fault resistance of 0.1 Ω and fault inception angle of 10° in Table 5, the PVC-based fault location result was the final fault section location, and the WSC-based and GA-based fault section location were not started. Otherwise, the second-stage fault section location based on WSC was started, such as in the case of the phase-phase short-circuit fault with fault resistance of 10 Ω and fault inception angle of 45° in Table 6. Using formula (7), the fault section location result was obtained. Then the fault section location reliability of the WSC-based fault location was calculated using formula (17). If $T_W > T_{Wth}$, the WSC-based fault location result was the final fault section location, and the GA-based fault section location was not started. Otherwise, such as in the case of the three-phase short-circuit fault with fault resistance of 10 Ω and fault inception angle of 90° in Table 5, the final fault section location result was provided by the third-stage GA-based fault section location.

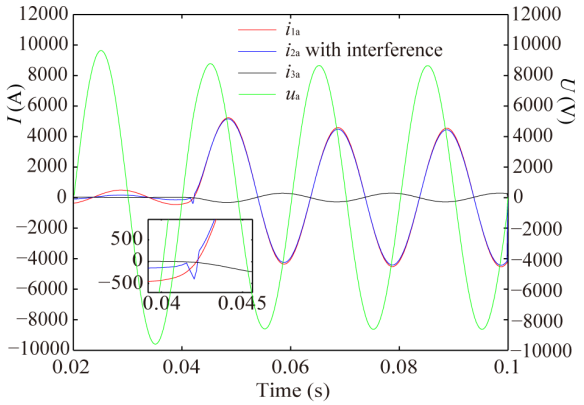

FIGURE 9. Fault currents and voltage of A-phase for phase-phase short circuit with interference.

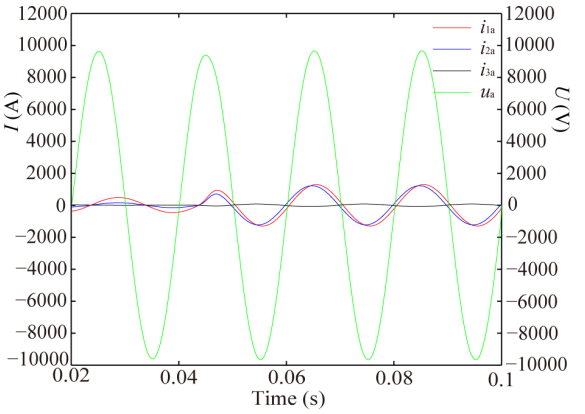

FIGURE 10. Fault currents and voltage of A-phase for phase-phase short circuit.

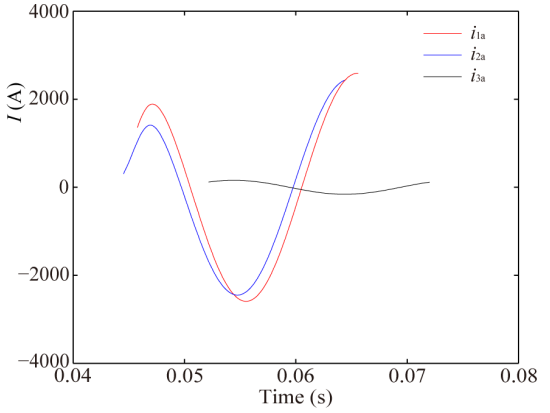

FIGURE 11. Fault currents with time lag of A-phase for phase-phase short circuit.

Thus, the fast and accurate fault section location was achieved.

D. SIMULATION VERIFICATION FOR SHORT-CIRCUIT FAULT WITH INTERFERENCE OR ASYNCHRONIZATION DATA

In the case in which the fault current i_{2a} was disturbed, the fault currents and voltage of the A-phase for three-phase short-circuit fault with fault inception angle (φ_f) of 45°, fault resistance (R_f) of 0.1 Ω, and fault position of 4.5 km are shown in Fig. 9. After the fault occurred, the first-stage fault section location based on PVC was put into operation. Using formula (3), the fault location parameters *PND* and *PNS* for the PVC-based fault section location could be calculated and the fault section location result was achieved, as shown in Table 5. Table 5 shows that the fault section was in section I, and the result was incorrect. Using formula (13), the PVC-based fault section location reliability was 0.5469 (less than 0.6), and the result of fault location was unreliable. Then the WSC-based fault section location was started. Using formula (6), we calculated the similarities and obtained the fault section location result using formula (7), as shown in Table 5. The fault section location result was correct. Using formula (17), the WSC-based fault section location reliability was 1 which was larger than 0.6, the result of fault section location was reliable. Thus, the fault section location result based on WSC was the final fault section location result (i.e., the fault section was in section II).

When the fault currents of upstream and downstream detection points were not synchronized, the reliability of fault section location was reduced, and the fault section location was incorrect. For example, Fig. 10 shows the initial fault currents and voltage of the A-phase when the phase-phase short-circuit fault with fault inception angle (φ_f) of 90°, fault resistance (R_f) of 10 Ω, and fault position of 4.5 km occurred. Because the fault current amplitude of the detection point D_3 was small, some inception fault current data were lost, resulting in data that were not synchronized, as shown in Fig. 11. First, the first-stage fault section location based on PVC was started. Using formula (3), the fault location parameters *PND* and *PNS* could be calculated, and the fault location was judged to be in section III, as shown in Table 6. The fault location result was incorrect. Using formula (13), the fault section location reliability of the PVC-based fault location was 0, and the result of fault location was unreliable. Then the second-stage fault section location based on WSC was started. Using formula (6), the fault location parameter ρ could be calculated, and the fault location was judged to be in section III, as shown in Table 6. The fault location result was incorrect. Using formula (17), the fault section location reliability of the WSC-based fault location was 0, and the result of fault location was unreliable. Finally, the third-stage fault section location was started. The fault section was judged to be in section II, which was the correct result.

To verify the advantage of rapidity of the multi-timescale-based fault section location, we conducted time-consuming tests of three fault section location methods. All of the simulations were performed in MATLAB2014a. The computer configuration was as follows: System: Windows 10 64-bit; CPU: Core i7-5500U @ 2.40 GHz; Memory: 8 GB. We wrote the corresponding the fault location programs of the three-stage fault location algorithms on the computer. After many tests, the average time consumption of the three fault section location methods was calculated, as shown in Table 7. Table 7 shows that the distributed fault location methods could realize fast fault location.

TABLE 7. Average time-consumption of the three fault section location methods.

Fault section location method	PVC	WSC	GA
Average time consumption (s)	0.0125	0.0232	1.652

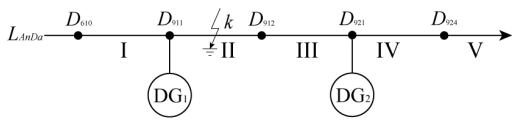

FIGURE 12. Structure of the feeder L_{AnDa}.

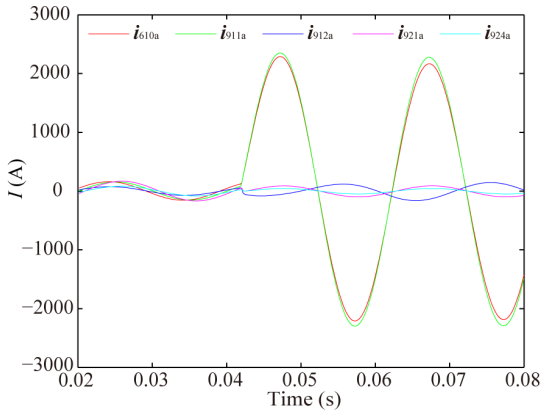

FIGURE 13. Fault currents of A-phase for field three-phase short circuit.

TABLE 8. PVC-based fault section location results for field three-phase short-circuit fault.

Section	Current	*PND*	*PNS*	D_{th}	Fault location result
I	i_{1a}, i_{2a}	0	128	64	Sound
	i_{1b}, i_{2b}	1	-89	44	
	i_{1c}, i_{2c}	-2	34	16	
II	i_{2a}, i_{3a}	114	14	50	Fault
	i_{2b}, i_{3b}	-74	-16	29	
	i_{2c}, i_{3c}	32	4	14	
III	i_{3a}, i_{4a}	-50	—	0	Sound
	i_{3b}, i_{4b}	29	—	0	
	i_{3c}, i_{4c}	-14	—	0	
VI	i_{4a}, i_{5a}	—	—	—	Sound
	i_{4b}, i_{5b}	—	—	—	
	i_{4c}, i_{5c}	—	—	—	
V	i_{5a}	—	—	—	Sound
	i_{5b}	—	—	—	
	i_{5c}	—	—	—	

The simulation results show that the multi-timescale-based fault section location has higher speed when the inception fault characteristics are significant and slower speed when the fault characteristics are weak. It can, however, ensure higher fault location accuracy.

VII. FIELD VERIFICATION

An actual feeder L_{AnDa} of a substation is shown in Fig. 12. The feeder starting detection point D_{610} used the line selection device to detect the current, and other detection points D_{911}, D_{912}, D_{921}, and D_{924} used SDU to detect the current. A three-phase short circuit fault between D_{912} and D_{921} occurred in July 2015. The A-phase fault currents all detection points are shown in Fig. 13. Table 8 shows the difference and sum of polarity values of fault current calculated at each detection point. According to the data in Table 8, using formula (3), SDU_{912} judged that three-phase short circuit fault occurred between D_{912} and D_{921}, and the fault location result was correct. According to formula (13), the reliability of first-stage location was $T_P = 1$, which was high, so the second-stage and third-stage fault location would not be started. We used another 120 groups of short-circuit fault data to verify the multi-timescale-based fault section location method. All fault section location results were correct. The PVC-based fault location results of 93 groups of data had high reliability, and the WSC-based fault location results of other 27 groups of data had high reliability. Therefore, the proposed fault location method based on multi-timescale was fast and effective.

VIII. CONCLUSION

In this study, we proposed a novel multi-timescale-based fault section location method for distribution networks. The proposed method can be applied to distribution lines with DG access. The following conclusions were obtained:

1. To meet the requirements of smart distribution networks for rapidity of fault location, we proposed two distributed fault section location methods: fault section location based on PVC and fault section location based on WSC. These fault location methods could be implemented by smart distributed units in parallel.
2. To achieve high-accuracy fault location, we constructed reliability functions of the distributed fault section location methods based on PVC and WSC. With the help of these fault location reliability functions, three kinds of fault section location based on PVC, WSC, and GA cooperated closely to realize fault section location based on multiple timescales.
3. The simulation results showed that the multi-timescale-based fault section location method could realize fast and accurate fault location in a distribution network with DG.

A single-phase-to-ground fault is always a difficult problem in fault section location because of its small amplitude of fault current and susceptibility to environmental conditions. The next step is to study single-phase-to-ground fault section location based on multiple timescales.

REFERENCES

[1] E. A. Reche, J. V. D. Sousa, D. V. Coury, and R. A. S. Fernandes, "Data mining-based method to reduce multiple estimation for fault location in radial distribution systems," *IEEE Trans. Smart Grid*, vol. 10, no. 4, pp. 3612–3619, Jul. 2019.
[2] G. Chen, M. Li, T. Xu, and M. Liu, "Study on technical bottleneck of new energy development," *Proc. CSEE*, vol. 37, no. 1, pp. 20–27, Jan. 2017.
[3] Q. Pang, L. Ye, H. Gao, X. Li, Y. Zheng, and C. He, "Penalty electricity price-based optimal control for distribution networks," *Energies*, vol. 14, no. 7, p. 1806, Mar. 2021.
[4] X. Wang, H. Zhang, F. Shi, Q. Wu, V. Terzija, W. Xie, and C. Fang, "Location of single phase to ground faults in distribution networks based on synchronous transients energy analysis," *IEEE Trans. Smart Grid*, vol. 11, no. 1, pp. 774–785, Jan. 2020.

[5] Y. Xiong, W. Yao, W. Chen, J. Fang, X. Ai, and J. Wen, "A data-driven approach for fault time determination and fault area location using random matrix theory," *Int. J. Electr. Power Energy Syst.*, vol. 116, Mar. 2020, Art. no. 105566.

[6] K. Yu, J. Zeng, X. Zeng, F. Xu, Y. Ye, and Y. Ni, "A novel traveling wave fault location method for transmission network based on directed tree model and linear fitting," *IEEE Access*, vol. 8, pp. 122610–122625, 2020.

[7] A. Farughian, L. Kumpulainen, and K. Kauhaniemi, "Earth fault location using negative sequence currents," *Energies*, vol. 12, no. 19, p. 3759, Sep. 2019.

[8] G. Manassero, S. G. Di Santo, and L. Souto, "Heuristic method for fault location in distribution feeders with the presence of distributed generation," *IEEE Trans. Smart Grid*, vol. 8, no. 6, pp. 2849–2858, Nov. 2017.

[9] M. A. Gabr, D. K. Ibrahim, E. S. Ahmed, and M. I. Gilany, "A new impedance-based fault location scheme for overhead unbalanced radial distribution networks," *Electr. Power Syst. Res.*, vol. 142, pp. 153–162, Jan. 2017.

[10] S. Shi, B. Zhu, A. Lei, and X. Dong, "Fault location for radial distribution network via topology and reclosure-generating traveling waves," *IEEE Trans. Smart Grid*, vol. 10, no. 6, pp. 6404–6413, Nov. 2019.

[11] Y. Xu, C. Zhao, S. Xie, and M. Lu, "Novel fault location for high permeability active distribution networks based on improved VMD and S-transform," *IEEE Access*, vol. 9, pp. 17662–17671, 2021.

[12] Y. Shi, T. Zheng, and C. Yang, "Reflected traveling wave based single-ended fault location in distribution networks," *Energies*, vol. 13, no. 15, p. 3917, Jul. 2020.

[13] H. Zhang, Z. Pan, and Z. Sang, "Injecting current based method for fault loca-tion in neutral isolated power system," *Autom. Electr. Power Syst.*, vol. 28, no. 3, pp. 64–66, Feb. 2004.

[14] M. Abad, M. García, N. E. Halabi, and D. López, "Network impulse response based-on fault location method for fault location in power distribution systems," *IET Gener., Transmiss. Distrib.*, vol. 10, no. 15, pp. 3962–3970, Nov. 2016.

[15] Y. Liu, X. Le, and X. Gu, "Synthesis matrix algorithm for fault section detec-tion and isolation in distribution system," *Electr. Power Autom. Equip.*, vol. 126, no. 3, pp. 38–41, Mar. 2006.

[16] T. Ma and L. Gao, "Fault location algorithm for active distribution network with multi micro-grids," *Power Syst. Prot. Control*, vol. 45, no. 7, pp. 64–68, Apr. 2017.

[17] Z. Wei, H. He, and Y. Zheng, "Advanced genetic algorithm for fault interval location in distribution network," *Proc. CSEE*, vol. 22, no. 4, pp. 127–130, Apr. 2002.

[18] J. Liang, T. Jing, H. Niu, and J. Wang, "Two-terminal fault location method of distribution network based on adaptive convolution neural network," *IEEE Access*, vol. 8, pp. 54035–54043, 2020.

[19] C. Zhang, X. Yuan, M. Shi, J. Yang, and H. Miao, "Fault location method based on SVM and similarity model matching," *Math. Probl. Eng.*, vol. 2020, Sep. 2020, Art. no. 2898479.

[20] Z. Jiao and R. Wu, "A new method to improve fault location accuracy in transmission line based on fuzzy multi-sensor data fusion," *IEEE Trans. Smart Grid*, vol. 10, no. 4, pp. 4211–4220, Jul. 2019.

[21] A. T. D. Perera, Z. Wang, V. M. Nik, and J.-L. Scartezzini, "Towards realization of an energy internet: Designing distributed energy systems using game-theoretic approach," *Appl. Energy*, vol. 283, Feb. 2021, Art. no. 116349.

[22] J. Sun, R. Chen, S. Cai, Q. Li, P. Zhao, and D. Dong, "A new fault location scheme for distribution system with distributed generations," *Power Syst. Technol.*, vol. 37, no. 6, pp. 1645–1650, Jun. 2013.

QINGLE PANG received the B.S. degree in automatic control engineering and the Ph.D. degree in control theory and control engineering from Shandong University, China, in 1994 and 2007, respectively. He is currently a Professor with the School of Information and Control Engineering, Qingdao University of Technology. His research interests include power system protection and control, smart grid technology, and operation optimization of power systems.

LIN YE received the B.E. degree in electrical engineering from the Qingdao University of Technology, Qingdao, China, in 2019, where he is currently pursuing the M.S. degree in control science and engineering. His research interests include power system protection and control and operation optimization of power systems.

HOULEI GAO was born in Shandong, China, in 1963. He received the B.Sc. and M.Sc. degrees in electrical power engineering from Shandong University, Jinan, China, in 1983 and 1988, respectively, and the Ph.D. degree from Tianjin University, Tianjin, China, in 1997. From 2004 to 2005, he was with the School of Electrical and Electronic Engineering, Queen's University Belfast, Belfast, U.K. He is currently a Professor with the School of Electrical Engineering, Shandong University. His research interests include power system protection, feeder automation, distributed generation, and digital substation.

XINIAN LI was born in Weifang, Shandong, China, in 1982. He received the B.Eng. degree in automation from Yantai University, Yantai, China, in 2006, the M.Eng. degree in control theory and control engineering from Northeastern University, Shenyang, China, in 2008, and the Ph.D. degree in control theory and control engineering from the China University of Mining and Technology, Beijing, China, in 2014.

From 2008 to 2011, he was an Electrical Engineer with Shanghai Baoshan Iron & Steel Company Ltd., Shanghai, China. Since 2014, he has been with Shandong Technology and Business University, Yantai. His research interests include harmonic filter, phase-locked loop, and power converter control.

YANGJIE WANG received the B.E. degree in automation from Anhui Polytechnic University, Anhui, China, in 2020. He is currently pursuing the M.S. degree in control science and engineering with the Qingdao University of Technology. His research interests include power system protection and control, fault detection, and control of intelligent distribution networks.

TONG CAO received the B.E. degree in electrical engineering from the Qingdao University of Technology, Qingdao, China, in 2021, where he is currently pursuing the M.S. degree in control science and engineering. His research interests include power system protection and control and operation optimization of power systems.